CHEMCATCHEM

DOI: 10.1002/cctc.200900223

Electro-Oxidation of Methanol on Pt–Ru Nanostructured Catalysts Electrodeposited onto Electroactivated Carbon Fiber Materials

Juan M. Sieben,* Marta M. E. Duarte, and C. E. Mayer[a]

The surface of different carbon substrates, such as glassy carbon (GC), graphite cloth (GC-10), graphite felt (GF-S2), and carbon fiber paper (CFP) was modified by electrochemical treatment to generate high concentrations of oxygenated functional groups. These activated carbons were used as substrates for the simultaneous electrodeposition of Pt and Ru by a double potentiostatic pulse program. The different catalyst/carbon systems were evaluated as electrodes for methanol oxidation in acid solution. Comparing the results for the oxidized and nonoxidized substrates, the oxidation of the different carbon materials prior to the catalyst deposition was found to lead to an increase in the electrode activity for methanol oxidation. This enhancement could be associated with a remarkable improvement of metal dispersion, reduction of particle size, and a higher active surface area of the catalyst. The electrodes prepared with oxidized graphite felt exhibited the greatest catalytic activity.

Introduction

Direct methanol fuel cells (DMFC) are amongst the most promising alternative energy sources for the near future, primarily to power electric vehicles and portable electronic devices, due to their high energy density, simple system, and the easy availability of liquid fuel.[1–3] Anodes for methanol oxidation in DMFC are porous electrodes comprising a carbon substrate over which a bimetallic Pt–Ru electrocatalyst is distributed in the form of small particles.[4] Several studies have shown that the intrinsic activity of the catalyst for methanol oxidation is determined by at least three factors: Ru concentration in the bimetallic catalyst, particle size, and carbon support surface properties.[5,6]

Carbon materials have been used as catalyst supports in many reactions involving organic compounds. They satisfy most of the necessary requirements for an appropriate support: chemical stability, high surface area, and adequate porosity. The chemical reactivity of carbon is due primarily to the presence of unsaturated bonds (active sites) at the edges of graphite-like hexagonal crystallites (graphene layers). The proportion of these active sites, relative to the inert carbon atoms within the graphene layers, increases as the surface area of the carbon material increases. Moreover, oxygen accumulation on active sites takes place even at room temperature, regardless of the nature of the carbon. Because of the varying amounts of surface oxygen functional groups, the carbon surface loses its inertness and becomes amphoteric.[6]

The anodic oxidation of carbonaceous materials in aqueous solution generates surface oxides consisting mainly of carboxylic and phenolic functionalities and three-dimensional bulk oxides.[7–9] The composition and quantity of these oxides can be controlled by an appropriate choice of current density and electrode potential as well as by the electrolyte solution.[10–12]

The presence of these surface oxides modifies the chemical and physical properties of the carbon, improving wettability, adsorption, and cation exchange capacity.[11,13] Furthermore, these surface oxides act as nucleation centers or anchoring sites, limiting the particle growth and improving the dispersion of metallic crystallites and the stability of the supported catalysts. It is necessary to understand the relationship between the active metal phase and the support in order to formulate and design new, better-performing catalysts for low-temperature fuel cells.

Herein, we report the preparation of bimetallic Pt–Ru catalysts by a double potentiostatic pulse program on different carbonaceous substrates, such as glassy carbon, graphite cloth, graphite felt, and carbon fiber paper. The influence of the anodic potentiostatic activation of the substrates on the morphological and structural characteristics of Pt–Ru catalysts and their activity for methanol oxidation is studied using scanning electron microscopy (SEM), X-ray diffraction (XRD), thermogravimetric analysis (TGA), and electrochemical techniques.

Experimental Section

Glassy carbon (GC) discs with an exposed geometric area of 0.07 cm^2 were used as reference substrate electrodes. Before Pt–Ru electrodeposition, the electrodes were polished to mirror with emery paper and alumina. Additionally, graphite cloth (GC-10, 203.4 $g\,m^{-2}$), graphite felt (GF-S2, 14.0 $g\,m^{-2}$), and carbon fiber

[a] Dr. J. M. Sieben, Prof. M. M. E. Duarte, Prof. C. E. Mayer
Instituto de Ingeniería Electroquímica y Corrosión (INIEC)
Universidad Nacional del Sur Av. Alem 1253 (B8000CPB)
Bahía Blanca, Argentina
Fax: (+54) 291-4595182
E-mail: jmsieben@uns.edu.ar

paper (CFP, 58.6 g m^{-2}) were also used as catalyst supports. The geometric area of these electrodes was 1 cm^2. The three-dimensional carbon supports were cleaned with acetone prior to use, and afterwards they were dried and impregnated with a diluted solution of $H_2[PtCl_6]$+$RuCl_3$ for 15 min.

Electrochemical measurements were carried out in a conventional glass cell at room temperature. The counter-electrode was a platinum foil separated from the working electrode compartment by a porous glass diaphragm. The reference electrode was a saturated calomel electrode (SCE, +0.241 V vs. RHE) located in a Luggin capillary. All of the potentials mentioned herein are referred to this electrode. Prior to electrochemical studies, the solutions were deaerated for 30 min with nitrogen. A PAR 273 A potentiostat was used to run the experiments. Conventional electrochemical techniques such as linear and cyclic voltammetry were applied to characterize supports and catalysts.[11]

The electrochemical pretreatment of the different carbon supports was performed by anodic potentiostatic polarization in 0.5 M H_2SO_4 at 2 V for 300 s followed by a linear cathodic potential sweep down to −0.6 V (scan rate = 1 mV s^{-1}).[12,15] After the pretreatment, nitrogen was bubbled through the acid solution for 15 min to eliminate oxygen traces in the electrolyte evolved during the pretreatment at 2 V. The charge involved in this reduction process was used as the reproducibility criterion of the carbon pretreatment. Values of 25.45 ± 0.85 mC cm^{-2}, 345.30 ± 1.25 mC cm^{-2}, 140.38 ± 1.42 mC cm^{-2}, 1,105.50 ± 2.85 mC cm^{-2} were determined for GC, GC-10, GF-S2 and CFP, respectively.

Catalyst electrodeposition was carried out from dilute aqueous solutions containing 2 mM H_2PtCl_6, 2 mM $RuCl_3$, and 0.5 M H_2SO_4. An inert nitrogen atmosphere was maintained over the electrolyte. Pt–Ru catalysts supported over different carbon substrates were prepared by chronoamperometry using a two-step process. The first potential step was fixed at −0.5 V for 5 s (t_1), followed by a second step at −0.2 V for 300 s (t_2), with the deposition under mass transfer control.[11]

After deposition, the electrodes were thoroughly rinsed with twice-distilled water. The different electrodes are designated by the catalyst plus the substrate, followed by the subscript "OX" if the substrate has been previously oxidized (e.g. Pt/GC_{OX}).

The morphology of the catalyst surface and the particle size were analyzed by SEM using a JEOL 100 microscope. Bulk compositional analysis of the Pt–Ru catalyst was performed using an X-ray detector for energy dispersive spectroscopy analysis (EDX). The structure of the electrodes was characterized by XRD using a Rigaku Dmax III C diffractometer using a monochromated CuKα source operated at 40 keV at a scan rate of 0.05 s^{-1}. TGA, to determine the extent of oxidation of the different carbon supports, was carried out using a Perkin–Elmer II TGA.

The active surface area (S) of the electrocatalysts was determined by copper underpotential deposition (Cu-UPD). Experimental details were described in a previous paper.[16] The loading of the catalysts was determined assuming 80% faradic efficiency for Pt^{+4} reduction under diffusion control.

The electrochemical oxidation of methanol was characterized by chronoamperometric experiments at 0.2 V, 0.3 V, and 0.4 V in 1 M CH_3OH+0.5 M H_2SO_4 solution at room temperature.[16] Catalytic activity is displayed in terms of current per unit of active surface area and current per mass of catalyst.

Results and Discussion

Characterization of the carbon substrates

Figure 1 shows cyclic voltammograms for the oxidized and nonoxidized materials in acid media. Each sample was examined before and after the oxidizing pretreatment. An anodic peak at 0.4 V and a cathodic peak at 0.3 V can be seen. These

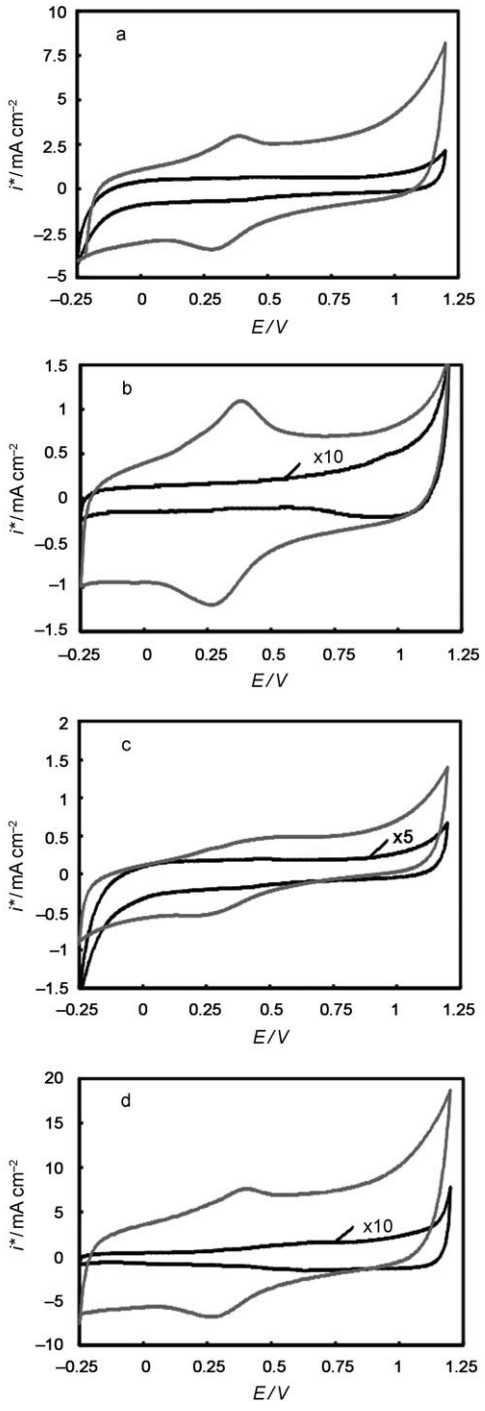

Figure 1. Cyclic voltammograms of nonoxidized (——) and oxidized (——) carbon substrates in 0.5 M H_2SO_4: a) GC; b) GC-10; c) GF-S2; d) CFP. $|dE/dt| = 50$ mV s^{-1}. i^* represents the current density per unit of geometric area.

peaks are characteristic of the presence of carbon surface oxide groups and they correspond to the quinone/hydroquinone redox reaction (Q/H_2Q).[11–15,17,18] The oxidative treatment of the carbon surface gives rise to the formation of surface acidic sites that influence the electrochemical interfacial state of the carbon surface and its double-layer properties.[19,20] Moreover, the carbon activation process in a sulfate solution increases the roughness of the substrate surface and leads to the formation of a great amount of anchoring sites for metal nucleation.[21] The presence of these oxygenated groups causes the increase in the current of the electrochemical double layer (Figure 1).

Figure 2 shows TGA curves for the carbon fiber materials, GC-10, GF-S2, and CFP, with and without previous oxidizing anodic treatment. The weight loss is due to the presence of oxygenated surface groups. Surface oxide groups decompose upon heating under an inert atmosphere to produce CO_2 for the most acidic groups (carboxyl, lactones and anhydrides) and CO for the least acidic groups (quinones, ethers, phenols, carbonyl, and hydroquinones).[21–23]

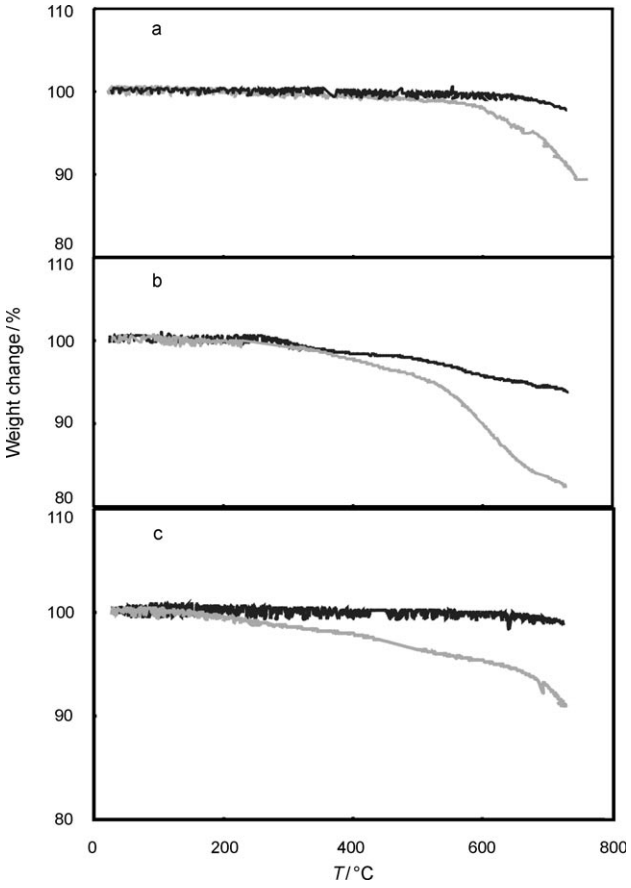

Figure 2. TGA curves of nonoxidized (——) and oxidized (——) carbon substrates: a) GC-10; b) GF-S2; c) CFP.

The TGA curves that correspond to the electrodes without anodic pretreatment show that GF-S2 carbonaceous material (Figure 2b) exhibits a higher degree of initial oxidation, probably caused by the manufacturing process, whereas GC-10 (Figure 2a) and CFP (Figure 2c) do not undergo an appreciable weight loss in the entire range of temperatures. In contrast, the curves of the electrodes that were oxidized anodically at 2 V show a greater loss in weight than those for electrodes without treatment, due to the high concentration of oxygenated groups. In the case of GC-10, the weight loss began at temperatures greater than 600 °C, whereas for GF-S2 and CFP the weight changes began at temperatures slightly above 400 °C.

The weight percentage loss was greater for GF-S2 and CFP than for GC-10, which indicates that both substrates are more readily oxidized. This phenomenon can be explained by the initial oxidation that takes place during the manufacturing process, and probably by the material macroscopic structural characteristics shown by the SEM images (Figure 3). Graphite cloth is formed by bundles of fibers, whereas, in graphite felt and carbon fiber paper, the fibers are separate and randomly distributed. In GC-10, the solution is more likely to flow around the bundles than through them since the space between the fibers is very limited. In contrast, in graphite felt and carbon fiber paper the solution is in a more efficient contact with the fibers since the interfibrous spaces are larger and uniformly distributed. The fiber surfaces in both GF-S2 and CFP are thus more easily accessible to electrochemical oxidation.

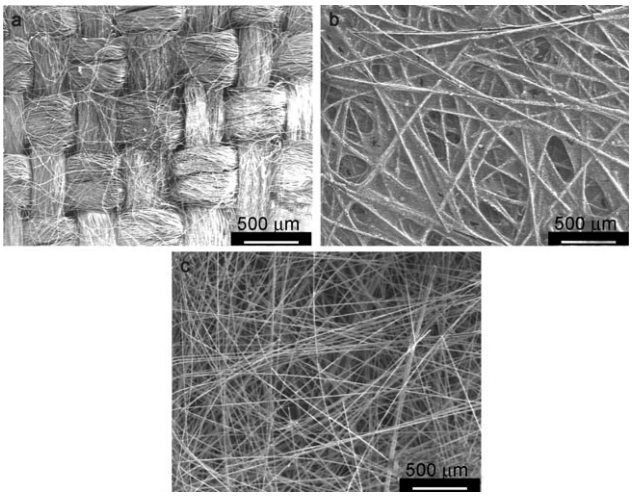

Figure 3. SEM images showing the macroscopic structure of the different carbon materials: a) GC-10; b) GF-S2; c) CFP.

Supported Pt–Ru catalyst morphology, structure, and composition

The EDX analysis of the Pt–Ru catalysts shows that Ru percentage in the samples prepared with untreated substrates is between 23 and 25 at.%, whereas lower Ru content (ca. 17 at.%) is determined in the electrodes prepared with pretreated substrates. Although the electrodeposition of platinum and ruthenium on electrochemically activated carbon electrodes is not fully understood, the difference in the composition of the bimetallic catalyst may be due to changes in

the way that platinum particles are deposited on the activated substrate. In other words, the observed behavior may be a consequence of several phenomena: 1) the interface is altered when the substrate is oxidized and this modification changes the real potential of the electrodes, modifying the conditions for platinum and ruthenium electrodeposition; 2) the kinetics of the Pt nucleation process may be accelerated by the presence of the oxygenated groups, limiting Ru nucleation; 3) the dispersion of Pt crystallites at the beginning of the deposition process can reduce the amount of deposited Ru (a geometric effect); 4) the electronic interaction between the Pt particles and the oxygenated surface groups may influence the nucleation of the Ru atoms. Nevertheless, it is not clear, at the moment, which is the predominant cause, and this will be the object of future study.

XRD patterns (Figure 4) revealed the bulk structure of the catalyst and the carbon support. Figure 4a and c show the diffraction patterns for Pt–Ru/GC-10 electrodes on a nonoxidized

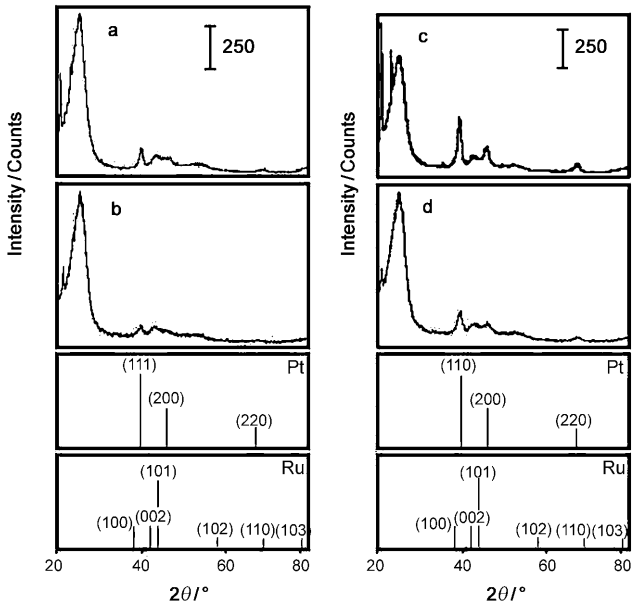

Figure 4. XRD diffractograms of the systems: a) Pt–Ru/GC-10b) Pt/GC-10; c) Pt–Ru/GC-10_{OX}; d)Pt/GC-10_{OX}. Platinum and ruthenium were deposited under the following conditions: $E_1 = -0.5$ V, $t_1 = 5$ s; $E_2 = -0.2$ V, $t_2 = 300$ s.

substrate and a substrate that had been oxidized in the conditions described previously, respectively. Figure 4b and d show the XRD patterns for Pt/GC-10 electrodes using nonoxidized and oxidized substrates, respectively. The corresponding diffractograms of GF-S2 and CFP electrodes present similar characteristics to those of the GC-10 electrodes.

The diffraction peaks corresponding to the carbon support are located at $2\theta \approx 25^\circ$, 42° and 54°.In contrast, the diffractograms of Pt–Ru catalysts show three peaks characteristic of face-centered cubic (fcc) crystalline structures at $2\theta \approx 40.1^\circ$, 47.3° and 68.5°, which are associated with the [111], [200], and [220] planes, respectively, indicating that the catalysts all have principally single-phase disordered structures (i.e. solid solutions). Compared with the reflections of the pure Pt catalysts (Figure 4b and 4d), the diffraction peaks for the bimetallic catalysts were slightly shifted to higher 2θ values. The slight shift of the diffraction peaks reveals the formation of an alloy involving the incorporation of Ru atoms into the fcc structure of Pt. It is important to note that no diffraction peaks appear that indicate the presence of either a pure Ru or Ru-rich hexagonal close-packed (hcp) phase.

The peak profiles in the XRD patterns of the catalysts were obtained by integration of the respective areas after peak deconvolution using the Marquardt algorithm.[24] Lattice constants of 3.922(±0.002) Å and 3.919(±0.003) Å were determined for Pt/GC-10 and Pt/GC-10_{OX}, respectively, in good agreement with 3.923 for pure Pt, whereas values of 3.891(±0.002) Å and 3.898(±0.004) Å were obtained for Pt–Ru/GC-10 and Pt–Ru/GC-10_{OX}, respectively. The slight difference in the lattice constants of the electrocatalysts deposited on nonoxidized and oxidized supports may either be due to the small size of the particles,[25] or a result of a Pt–support interaction.[26] In addition, the ratio between [111] and [220] areas does not change significantly in these samples, indicating an absence of any preferential orientation.

From the values of the lattice parameters, the atomic fraction of Ru in the Pt–Ru alloy can be assessed, assuming that the Pt–Ru lattice parameter of the supported bimetallic alloy follows the Vegards' law [Eq. (1); a = lattice parameter, X = atomic fraction].

$$a_{Pt} = a_{Pt-Ru} - 0.124 X_{Ru} \quad (1)$$

The values obtained by XRD (Table 1) indicate a nominal Ru content of the Pt–Ru catalysts that agrees with the EDX results.

Table 1. Parameters of Pt and Pt–Ru catalysts electrodeposited on carbon fiber cloth. Data obtained from XRD, EDX and SEM analysis.

Electrode	d_c[a] [nm]	d_p[b] [nm]	$X_{Ru(EDX)}$[c] (±0.3)	$X_{Ru(XRD)}$[c] (±0.4)
Pt/GC-10	8	50	–	–
Pt/GC-10_{OX}	6	20	–	–
Pt–Ru/GC-10	5	70	0.25	0.27
Pt–Ru/GC-10_{OX}	4	50	0.17	0.16

[a] d_c = crystallite diameter (±0.3 nm) determined from Debye–Scherrer equation; [b] d_p = average particle diameter (±5 nm) determined from SEM images; [c] $X_{Ru(EDX)}$ and $X_{Ru(XRD)}$ = Ru content determined by EDX and XRD, respectively.

Debye–Scherrer's equation[27] was used to estimate the average Pt–Ru crystallite size from the broadening of the Pt [111] and [220] diffraction peaks centered around $2\theta = 40.2^\circ$ and 68.3°. The estimated values (Table 1) agree with those obtained by Coutanceau et al.[28]

Figure 5 shows SEM micrographs of Pt–Ru deposits on different substrates. Images of deposits on glassy carbon samples (not shown) appear similar to those observed on the other electrodes. In general, particles with globular shape are

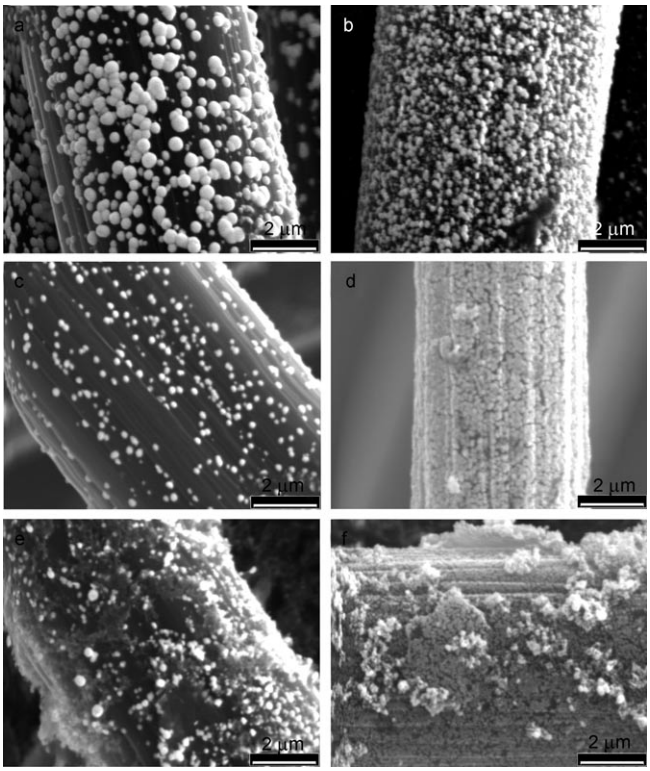

Figure 5. Top-view SEM images (12000× magnification) showing the Pt–Ru deposit on: a) GC-10; b) GC-10_{OX}; c) GF-S2; d) GF-$S2_{OX}$; e) CFP; f) CFP_{OX}. Platinum and ruthenium were deposited under the following conditions: $E_1 = -0.5$ V, $t_1 = 5$ s; $E_2 = -0.2$ V, $t_2 = 300$ s,

observed. The size of the catalyst particles depends on the pretreatment and the type of substrate. Crystallites are smaller and more homogenously distributed when GC-10 and GF-S2 substrates have been previously oxidized (Table 2). In addition, the oxidative treatment leads to a dramatic increase in the amount of Pt–Ru particles. In contrast, bigger, more irregular particles can be observed on the CFP substrate, although on these electrodes the favorable influence of the pretreatment on size and distribution is evident. These images indicate that the oxidation of the support leads to changes in the Pt–Ru particle size and dispersion.

Table 2. Parameters of nanostructured Pt–Ru/Carbon supported electrodes showing the influence of the oxidative pretreatment.

Substrate	d_p [nm]	$A^{[a]}$ (±0.3)	$S_w^{[b]}$ [$m^2 g^{-1}$]
GC	–	7.3	51.9
GC_{OX}	–	13.6	57.1
GC-10	70	61.4	89.8
GC-10_{OX}	50	92.6	117.1
GF-S2	65	24.0	68.7
GF-$S2_{OX}$	45	46.1	113.5
CPF	100	9.4	33.0
CFP_{Ox}	70	17.3	46.4

[a] A = active surface area per unit of geometric area. [b] S_w = specific surface area (±0.7 $m^2 g^{-1}$).

The samples were also examined with SEM microscopy and EDX analysis after electrochemical tests and no changes in particle morphology and phase composition were observed.

XRD patterns and SEM images were compared for both Pt–Ru/GC-10_{OX} and Pt–Ru/GC-10 electrodes. The XRD patterns showed particle diameters to be between 5 and 8 nm, whereas, in the SEM images, particles with sizes ranging from 50 to 70 nm were observed, establishing that the Pt–Ru particles observed by SEM were, in fact, agglomerates comprising small nanometric particles. The amount of particles forming each agglomerate may be related to Ru content and to the oxidation state of the carbon surface.

From the specific surface area values of the catalysts (S_w; Table 2), it can be seen that S_w was significantly affected by the type of carbon material on which the catalyst was deposited. Moreover, the specific surface area increased by a factor of approximately two when the support was oxidized. The metal–support interaction thus plays an important role by influencing the size, dispersion, and chemical state of the catalyst particles.

Electrochemical studies

For comparison, Pt–Ru electrodes were examined by cyclic voltammetry at a sweep rate of 10 $mV s^{-1}$ in the potential range between −0.25 V and +0.5 V in 0.5 M H_2SO_4 solution. The anodic limit was set to 0.5 V to prevent the formation of inactive ruthenium oxides and to minimize the effect of the electrochemical treatment on the deposit structure.

Typical voltammograms (Figure 6) show a remarkable increase in the current when oxidized substrate electrodes are compared with those prepared with the nonoxidized substrate. This behavior may be associated with the type and surface density of the electroactive O-containing groups developed during the oxidative treatment.

Peaks corresponding to the Q/H_2Q couple reaction are visible in the voltammograms of the electrodes formed from highly oxidized substrates, in addition to the peaks for adsorption and desorption of hydrogen (Figure 6b). The higher coulombic charge of the hydrogen adsorption/desorption zone is related to an increase in the active surface area of the catalyst due to better particle distribution, lower particle size and greater amount of catalyst particles deposited when the carbon material is electrochemically oxidized.

The electrocatalytic behavior of the electrodes prepared in this work was evaluated by potentiostatic experiments in the potential region that is relevant for methanol oxidation in DMFC (Table 3). The resultant chronoamperometric curves (Figure 7) show a very high initial catalyst activity, which rapidly decays to a much lower value within seconds. This current decay has previously been reported for a Pt–Ru catalyst at different temperatures and methanol concentrations.[29,30] The main cause of the current decay is the blocking of active sites by poisoning species. Chemisorption of methanol gives rise to the adsorption of CHO and CO intermediates with the former detected at short adsorption times and low potentials.[30]

The influence of the substrate on catalyst activity is assessed as a function of the current density per unit mass of catalyst

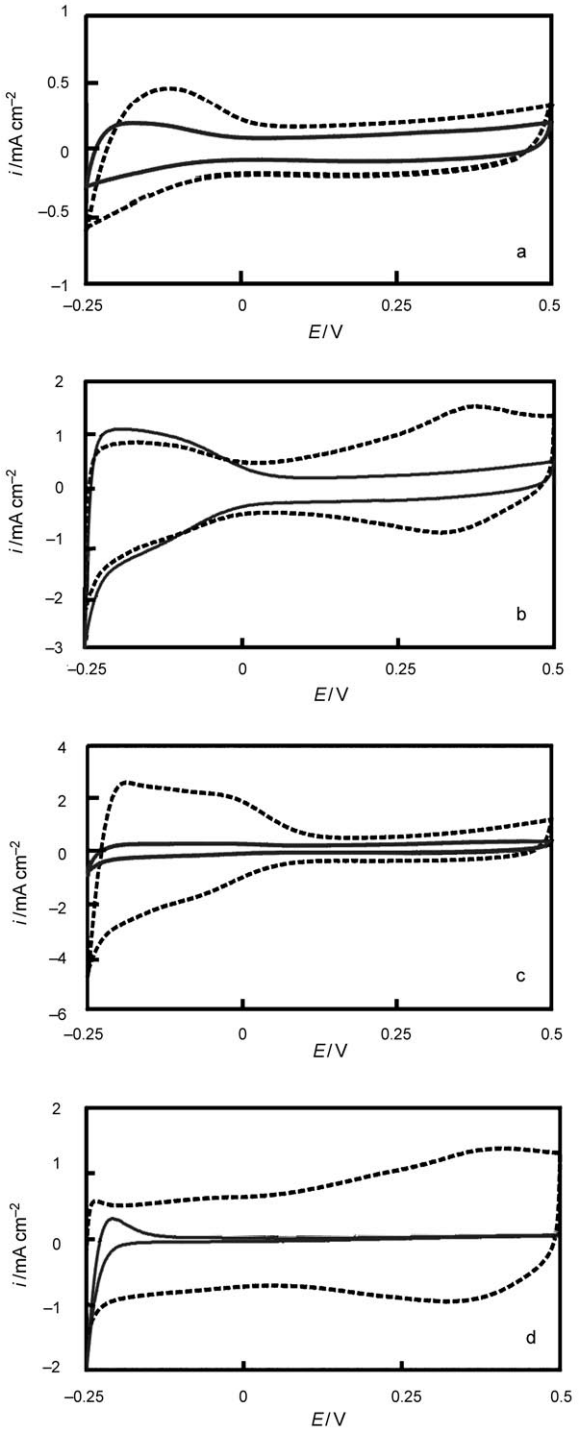

Figure 6. Cyclic voltammograms of the Pt–Ru particles on the nonoxidized (——) and oxidized (-----) carbon substrates in 0.5 M H_2SO_4: a) GC; b) GC-10; c) GF-S2; d) CFP. $|dE/dt| = 10\ mV\,s^{-1}$, $T = 25\,^{\circ}C$. Platinum and ruthenium were deposited under the following conditions: $E_1 = -0.5$ V, $t_1 = 5$ s; $E_2 = -0.2$ V, $t_2 = 300$ s.

(i_m) and per unit of active surface area (i). The electrodes prepared from oxidized substrates exhibit greater catalytic activity for methanol oxidation than those from nonoxidized substrates (Figure 7 and Table 3). This behavior can be attributed to the more uniform distribution of metals on the substrate

Table 3. Catalytic activity of nanostructured Pt–Ru/Carbon supported electrodes showing the influence of the oxidative pretreatment. Data taken from quasi-stationary experiments (Figure 7).

Substrate	$i^{[a]}$ [$\mu A\,cm^{-2}$]			$i_w^{[b]}$ [$A\,g^{-1}$]		
	0.2 V	0.3 V	0.4 V	0.2 V	0.3 V	0.4 V
GC	14	21	30	7.3	10.9	15.6
GC_{OX}	25	32	46	14.3	18.3	26.3
GC-10	28	36	41	25.1	32.3	36.8
GC-10_{OX}	38	45	67	44.5	52.7	78.5
GF-S2	50	76	91	34.4	52.2	62.5
GF-$S2_{OX}$	79	101	135	89.7	114.6	153.2
CPF	8	12	20	2.6	4	6.6
CFP_{Ox}	18	25	38	8.4	11.6	17.6

[a] i = current density per unit of active surface area. [b] i_m = current density per unit of catalyst load.

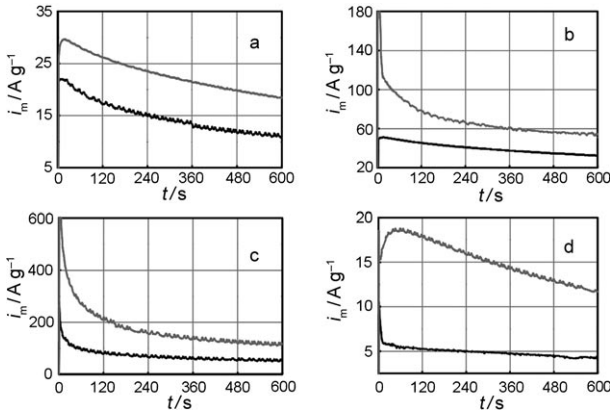

Figure 7. Chronoamperometric response at 0.3 V of methanol oxidation on Pt–Ru catalysts electrodeposited on the nonoxidized (——) and oxidized (——) substrates at room temperature: a) GC; b) GC-10; c) GF-S2; d) CFP. Platinum and ruthenium were deposited under the following conditions: $E_1 = -0.5$ V, $t_1 = 5$ s; $E_2 = -0.2$ V, $t_2 = 300$ s.

surface, the presence of smaller particles than those obtained with the nonoxidized materials, and the greater number of catalyst particles. The presence of acid surface groups promotes a more homogeneous dispersion and produces an increase in both the mass activity and the intrinsic activity. In addition, the increase in the hydrophilicity of the carbon materials facilitates the arrival of the metal ions to the electrode surface, increasing catalyst load.

Some differences in the catalytic performance of the electrodes are expected, as a consequence of changes in the alloy composition. The lower Ru content on the Pt–Ru/GC-10_{OX} electrode probably has some effect on the catalyst activity. When Ru content exceeded 20 at.% the number of surface sites available for methanol adsorption decreased reducing the activity of the catalyst. This result can be easily explained assuming a random distribution of Pt and Ru in the surface, as was recently outlined by Hoster et al.[31]

The catalytic performance of Pt–Ru/GF-$S2_{OX}$ in methanol oxidation was evaluated and compared with those reported in the literature. In most cases, direct comparison was difficult because the experimental conditions reported in the literature

for electrochemical evaluation of the catalytic activity of Pt–Ru/C are rather varied. Even so, the catalysts prepared in this work are known to offer comparable performances with commercial catalysts, as well as those previously reported.[32–48]

The competitiveness of the home-made catalysts can be associated with their pronounced defective structure, that is, high concentration of intergrain boundaries and nanopores. The presence of surface defects seems to be a *sine qua non* condition for achieving high catalytic activity, as was explained by Hoster et al.[49] Therefore, a qualitative explanation may be given on the basis of the differences in the surface structure of the electrodes prepared by the double step program. Electrodeposition of noble metals on carbon supports is known to occur by a three-dimensional nucleation and growth mechanism.[50] Generally, primary nucleation on carbon is followed by secondary nucleation on the predeposited Pt surface, except when short potential pulses are employed.[51] This behavior may be explained by considering the higher concentration of nucleation centers on the Pt surface compared to carbon. The result of secondary nucleation is formation of complex micro- and nanograined Pt structures.[52] Furthermore, on an atomically smooth HOPG surface, formation of particle agglomerates may also occur through migration and coalescence of Pt nanoparticles favored by weak interaction of Pt with the HOPG substrate. Therefore, Gloaguen et al.[50] and Zoval et al.[51] concluded that Pt electrodeposition on HOPG takes place by formation of particles 10–20 nm in diameter and, as the deposition time increases, subsequent surface diffusion results in the agglomeration of individual nanoparticles. The home-made catalysts are formed by agglomerates composed of nanosized metal grains interconnected at grain boundaries, resulting in the formation of multigrained structures. These discontinuities in the crystal planes may act in a similar manner to low-coordinated sites (steps and kinks) on single-crystalline and other extended surfaces,[52] which exhibit very high catalytic activity for methanol oxidation. Metal atoms in the proximity of grain boundaries usually have a decreased number of near neighbors in the first coordination shell and thus are expected to bind adsorbates and catalyze bond-breaking reactions, such as methanol dissociative chemisorption.[53]

In contrast, catalysts prepared by chemical techniques usually exhibit particle sizes between 2 and 5 nm. Takasu et al. reported the low activity of small particles in methanol oxidation,[54] and attributed it to the 'negative' particle size effect; since small Pt–Ru particles are more susceptible to poisoning. This conclusion is supported by the evidence presented by Mukerjee et al.[55] In this investigation smaller particles (<5 nm) with their higher proportion of low-coordination sites (greater number of surface sites with Pt d-band vacancies) adsorbs species such as H, OH and CO more strongly. Moreover, as noted previously, the homogeneous mixing of the two metals at the atomic scale and the ruthenium content in the solid solution are expected to be very important factors.[31]

Furthermore, another reason that can be put forward to explain the lesser activity of catalysts synthesized by chemical methods may be related to the nature of Pt–Ru species in the catalyst surface. Analysis of the catalysts by photoelectron spectroscopy provided evidence of the presence of Pt, Pt^{II}, and Pt^{IV} species in most of the catalysts prepared by chemical methods.[35] The presence of oxidized Pt species, such as PtO and PtO_2, in these Pt–Ru supported catalysts would contribute to their lesser activity due to a reduction of the available sites for methanol adsorption.

In addition, the presence of functional groups can contribute to improved electrode performance, since oxygenated functional groups strongly affect the behavior of catalyst.[56] Electron transfer between the oxygen atoms on the support and metal particles leads to enhanced electron density of the metal particles. Interactions at the metal–support interface decrease the adsorption strength of methanolic residues, that is, CO adsorption energy has been found to decrease on Pt/TiO_2 and Ni/TiO_2 due to electronic interactions.[57] Besides, higher concentration of oxidized groups on the surface of GC-10 could facilitate the accessibility of methanol to the electroactive surface and participate in the oxidation of the absorbed intermediate species formed in alcohol dissociation.

Conclusions

The combination of electrochemical oxidation of carbon substrates and electrodeposition by a double potentiostatic pulse program was used to prepare Pt–Ru bimetallic catalysts for methanol oxidation. The oxidation of the different carbon substrates prior to the catalyst deposition, led to a remarkable improvement in the deposit dispersion, a reduction in the particle size, and a higher active surface area of the catalyst. When the activity of the catalysts deposited on the different substrates was compared, the electrodes prepared with oxidized graphite felt exhibited the greater catalytic activity for methanol oxidation, both intrinsic and per mass unit, which can be attributed to the open material structure that allowed a more homogeneous distribution of deposits on the substrate surface, and the presence of smaller particles creating a higher number of active sites. These results may constitute an important contribution for the selection of activated carbons for use as electrode materials.

Acknowledgements

This work was supported by ANPCYT Grant N° 10-11133L, CIC and SECyT UNS, Argentina. J.M.S. acknowledges CONICET and wishes to thank Dr. G. Mas and Dr. M. Villar for their assistance in the XRD and TGA measurements, respectively.

Keywords: carbon · electrocatalysis · oxidation · platinum · ruthenium

[1] A. S. Aricò, S. Srinivasan, V. Antonucci, *Fuel Cells* **2001**, *1*, 133 – 161.
[2] T. Iwasita in *Handbook of Fuel Cells Fundamentals, Technology and Applications, Vol. 2* (Eds.: W. Vielstich et al.), Wiley, New York, **2003**, p. 603.
[3] H. Liu, Ch. Song, L. Zhang, J. Zhang, H. Wang, D. P. Wilkinson, *J. Power Sources* **2006**, *155*, 95 – 110.
[4] M. Watanabe, M. Uchida, S. Motoo, *J. Electroanal. Chem.* **1987**, *229*, 395 – 406.

[5] P. A. Attwood, B. D. McNicol, R. T. Short, *J. Appl. Electrochem.* **1980**, *10*, 213 – 222.
[6] M. Cerro-Alarcón, A. Maroto-Valiente, I. Rodríguez-Ramos, A. Guerrero-Ruiz, *Carbon* **2005**, *43*, 2711 – 2722.
[7] J. P. Randin in *Encyclopedia of Electrochemistry of the Elements, Vol. 7* (Ed.: J. Bard), Marcel Dekker, New York, **1976**, p. 22.
[8] H. Olender, W. E. O'Grady, H. S. Isaacs, S. Srinivasan, A. C. C. Tseung, *J. Appl. Electrochem.* **1982**, *12*, 135 – 145.
[9] V. M. Jovanović, S. Terzić, A. V. Tripković, K. Dj. Popović, J. L. Lović, *Electrochem. Commun.* **2004**, *6*, 1254 – 1258.
[10] J. H. Marsh, S. W. Orchard, *Carbon* **1992**, *30*, 895 – 901.
[11] M. M. E. Duarte, A. S. Pilla, J. M. Sieben, C. E. Mayer, *Electrochem. Commun.* **2006**, *8*, 159 – 164.
[12] F. Gloaguen, J. M. Léger, C. Lamy, *J. Appl. Electrochem.* **1997**, *27*, 1052 – 1060.
[13] P. L. Antonucci, V. Alderucci, N. Giordano, D. L. Cocke, H. Kim, *J. Appl. Electrochem.* **1994**, *24*, 58 – 65.
[14] M. M. E. Duarte, C. Mayer, *An. Asoc. Quim. Argent.* **1997**, *85*, 27 – 35.
[15] M. M. E. Duarte, A. S. Pilla, P. M. Taberner, C. E. Mayer, *An. Asoc. Quim. Argent.* **1993**, *81*, 415 – 430.
[16] J. M. Sieben, M. M. E. Duarte, C. E. Mayer, *J. Appl. Electrochem.* **2008**, *38*, 483 – 490.
[17] K. Kinoshita, J. A. S. Bett, *Carbon* **1974**, *12*, 525 – 533.
[18] J. Maruyama, I. Abe, *Electrochim. Acta* **2001**, *46*, 3381 – 3386.
[19] M. Musameh, N. S. Lawrence, J. Wang, *Electrochem. Commun.* **2005**, *7*, 14 – 18.
[20] C. A. Leon y Leon, L. R. Radovic, *Chemistry and Physics of Carbon, Vol. 24*, Marcel Dekker, New York, **1994**.
[21] A. Dekanski, J. Stevanović, R. Stevanović, B. Ž. Nikolić, V. M. Jovanović, *Carbon* **2001**, *39*, 1195 – 1205.
[22] O. V. Cherstiouk, P. A. Simonov, E. R. Savinova, *Electrochim. Acta* **2003**, *48*, 3851 – 3860.
[23] K. H. Kangasniemi, D. A. Condit, T. D. Jarvi, *J. Electrochem. Soc.* **2004**, *151*, E125 – E132.
[24] D. W. Marquardt, *SIAM J. Appl. Math.* **1963**, *11*, 431 – 441.
[25] C. Roth, M. Gotees, H. Fuess, *J. Appl. Electrochem.* **2001**, *31*, 793 – 798.
[26] A. K. Shukla, A. S. Arico, K. M. El Khatib, H. Kim, P. L. Antonucci, V. Antonucci, *Appl. Surf. Sci.* **1999**, *137*, 20 – 29.
[27] A. L. Patterson, *Phys. Rev.* **1939**, *56*, 978 – 982.
[28] C. Coutanceau, A. F. Rakotondrainibe, A. Lima, E. Garnier, S. Pronier, J.-M. Léger, C. Lamy, *J. Appl. Electrochem.* **2004**, *34*, 61 – 66.
[29] H. A. Gasteiger, N. M. Marković, P. N. Ross Jr. , E. J. Cairns, *J. Phys. Chem.* **1993**, *97*, 12020 – 12029.
[30] H. A. Gasteiger, N. M. Marković, P. N. Ross, E. J. Cairns, *J. Electrochem. Soc.* **1994**, *141*, 1795 – 1803.
[31] H. Hoster, T. Iwasita, E. Baumgärtner, W. Vielstich, *Phys. Chem. Chem. Phys.* **2001**, *3*, 337 – 346.
[32] F. J. Rodríguez-Nieto, T. Y. Morante-Catacora, C. R. Cabrera, *J. Electroanal. Chem.* **2004**, *571*, 15 – 26.
[33] J. L. Gómez de La Fuente, M. V. Martínez-Huerta, S. Rojas, P. Terreros, J. L. G. Fierro, M. A. Peñas, *Carbon* **2005**, *43*, 3002 – 3005.
[34] Z. Liu, X. Y. Ling, J. Y. Lee, X. Su, L. M. Gan, *J. Mater. Chem.* **2003**, *13*, 3049 – 3052.
[35] J. L. Gómez de La Fuente, M. V. Martínez-Huerta, S. Rojas, P. Terreros, J. L. G. Fierro, M. A. Peña, *Catal. Today* **2006**, *116*, 422 – 432.
[36] J. Prabhuram, T. S. Zao, Z. K. Tang, R. Chen, Z. X. Liang, *J. Phys. Chem. B* **2006**, *110*, 5245 – 5252.
[37] T. T. Cheng, E. L. Gyenge, *J. Appl. Electrochem.* **2007**, *38*, 51 – 62.
[38] C. Bock, M. A. Blakely, B. MacDougall, *Electrochim. Acta* **2005**, *50*, 2401 – 2414.
[39] L. S. Sarma, T. D. Lin, Y.-W. Tsai, J. M. Chen, B. J. Hwang, *J. Power Sources* **2005**, *139*, 44 – 54.
[40] L. Xiong, A. Manthiram, *Solid State Ionics* **2005**, *176*, 385 – 392.
[41] A. O. Neto, R. R. Dias, M. M. Tusi, M. Linardi, E. V. Spinacé, *J. Power Sources* **2007**, 166, 87 – 91.
[42] S. Kim a, S.-J. Park, *Solid State Ionics* **2008**, *178*, 1915 – 1921.
[43] T. Vidaković, M. Christov, K. Sundmacher, K. S. Nagabhushana, W. Fei, S. Kinge, H. Bönnemann, *Electrochim. Acta* **2007**, *52*, 277 – 2284.
[44] I.-S. Park, K.-W. Park, J.-H. Choi, C. R. Park, Y.-E. Sung, *Carbon* **2007**, *45*, 28 – 33.
[45] P. Sivakumar, V. Tricoli, *Electrochim. Acta* **2006**, *51*, 1235 – 1243.
[46] J. W. Guo, T. S. Zhao, J. Prabhuram, R. Chen, C. W. Wong, *Electrochim. Acta* **2005**, *51*, 754 – 763.
[47] Q. Lu, B. Yang, L. Zhuang, J. Lu, *J. Phys. Chem. B* **2005**, *109*, 1715 – 1722.
[48] M.-C. Tsai, T.-K. Yeh, C.-H. Tsai, *Electrochem. Commun.* **2006**, *8*, 1445 – 1452.
[49] H. E. Hoster, A. Bergbreiter, P. M. Erne, T. Hager, H. Rauscher, R. J. Behm, *Phys. Chem. Chem. Phys.* **2008**, *10*, 3812 – 3823.
[50] F. Gloaguen, J. M. Léger, C. Lamy, A. Marmann, U. Stimming, R. Vogel, *Electrochim. Acta* **1999**, *44*, 1805 – 1816.
[51] J. V. Zoval, J. Lee, S. Gorer, R. M. Penner, *J. Phys. Chem. B* **1998**, *102*, 1166 – 1175.
[52] A. N. Gavrilov, E. R. Savinova, P. A. Simonov, V. I. Zaikovskii, S. V. Cherepanova, G. A. Tsirlina, V. N. Parmon, *Phys. Chem. Chem. Phys.* **2007**, *9*, 5476 – 5489.
[53] O. V. Cherstiouk, A. N. Gavrilov, L. M. Plyasova, I. Y. Molina, G. A. Tsirlina, E. R. Savinova, *J. Solid State Electrochem.* **2008**, *12*, 497 – 509.
[54] Y. Takasu, H. Itaya, T. Iwazaki, R. Miyoshi, T. Ohnuma, W. Sugimoto, Y. Murakami, *Chem. Commun.* **2001**, *2001*, 341 – 342.
[55] S. Mukerjee, J. McBreen, *J. Electroanal. Chem.* **1998**, *448*, 163 – 171.
[56] O. A. Petrii, *J. Solid State Electrochem.* **2008**, *12*, 609 – 642.
[57] X. E. Verykios in *Catalysis and Electrocatalysis at Nanoparticles Surfaces* (Eds.: A. Wieckowski, E. R. Savinova, C. G. Vayenas), Marcel Dekker, New York, **2003**, Chap. 20, p. 748.

Received: August 27, 2009
Revised: October 6, 2009
Published online on November 24, 2009

